R. E., Isaacs, N. W., Reynolds, C. D., Sakabe, K., Sakabe, N., & Vijayan, N. M. (1988) *Philos. Trans. R. Soc. London, B 319*, 369-456.
Bentley, G. A., Dodson, E. J., Dodson, G. G., Hodgkin D. C., & Mercola, D. A. (1976) *Nature 261*, 166-168.
Brader, M. L., & Dunn, M. F. (1990) *J. Am. Chem. Soc. 112*, 4585-4587.
Brader, M. L., Kaarsholm, N. C., & Dunn, M. F. (1990) *J. Biol. Chem. 265*, 15666-15670.
Brader, M. L., Kaarsholm, N. C., Lee, R. W.-K., & Dunn, M. F. (1991) *Biochemistry 30*, 6636-6645.
Bunnett, J. F. (1974) *Techniques of Chemistry*, Vol. 4, Part I, pp 390-395, Wiley Interscience, New York.
Cotton, F. A., & Wilkinson, G. (1972) in *Advanced Inorganic Chemistry*, 3rd ed., p 885, Wiley Interscience, New York.
De Graaff, R. A. G., Lewit-Bentley, A., & Tolley, S. P. (1981) in *Structural Studies on Molecules of Biological Interest* (Dodson, G., Glusker, J. P., & Sayre, D., Eds.) pp 547-556, Clarendon Press, Oxford.
Derewenda, U., Derewenda, Z., Dodson, E. J., Dodson, G. G., Reynolds, C. G., Smith, G. D., Sparks, C., & Swensen, D. (1989) *Nature 338*, 594-596.
Kaarsholm, N. C., Ko, H.-C., & Dunn, M. F. (1989) *Biochemistry 28*, 4427-4435.
Koerber, S. C., MacGibbon, A. K. H., Dietrich, H., Zeppezauer, M., & Dunn, M. F. (1983) *Biochemistry 22*, 3424-3431.
Porter, R. R. (1953) *Biochem. J. 53*, 320-328.
Reinscheidt, H., Strassburger, W., Glatter, U., Wollmer, A., Dodson, G. G., & Mercola, D. A. (1984) *Eur. J. Biochem. 142*, 7-14.
Roy, M., Brader, M. L., Lee, R. W.-K., Kaarsholm, N. C., Hansen, J. F., & Dunn, M. F. (1989) *J. Biol. Chem. 264*, 19081-19085.
Smith, G. D., Swenson, D. C., Dodson, E. J., Dodson, G. G., & Reynolds, C. D. (1984) *Proc. Natl. Acad. Sci. U.S.A. 81*, 7093-7097.
Wollmer, A., Rannefeld, B., Johansen, B. R., Hejnaes, K. R., Blaschmidt, P., & Hansen, F. B. (1987) *Biol. Chem. Hoppe-Seyler 368*, 903-912.

Fluorescence, CD, Attenuated Total Reflectance (ATR) FTIR, and ^{13}C NMR Characterization of the Structure and Dynamics of Synthetic Melittin and Melittin Analogues in Lipid Environments†

Arthur J. Weaver,‡,§ Marvin D. Kemple,*,‖ Joseph W. Brauner,⊥ Richard Mendelsohn,⊥ and Franklyn G. Prendergast*,‡

Department of Biochemistry and Molecular Biology, Mayo Foundation, Rochester, Minnesota 55905, Department of Physics, Indiana University-Purdue University at Indianapolis, Indianapolis, Indiana 46205-2810, and Department of Chemistry, Rutgers University, Newark, New Jersey 07102

Received September 16, 1991

ABSTRACT: The structure and dynamics of synthetic melittin (MLT) and MLT analogues bound to monomyristoylphosphatidylcholine micelles, dimyristoylphosphatidylcholine vesicles, and diacylphosphatidylcholine films have been investigated by fluorescence, CD, attenuated total reflectance (ATR) FTIR, and ^{13}C NMR spectroscopy. All of these methods provide information about peptide secondary structure and/or about the environment of the single tryptophan side chain in these lipid environments. ATR-FTIR data provide additional information about the orientation of helical peptide segments with respect to the bilayer plane. Steady-state fluorescence anisotropy, fluorescence lifetime, and ^{13}C NMR relaxation data are used in concert to provide quantitative information about the dynamics of a single ^{13}C-labeled tryptophan side chain at position 19 in lipid-bound MLT, and at positions 17, 11, and 9, respectively, in lipid-bound MLT analogues. Peptide chain dynamics are probed by NMR relaxation studies of $^{13}C\alpha$-labeled glycine incorporated into each of the MLT peptides at position 12. The cumulative structural and dynamic data are consistent with a model wherein the N-terminal α-helical segment of these peptides is oriented perpendicular to the bilayer plane. Correlation times for the lysolipid-peptide complexes provide evidence for binding of a single peptide monomer per micelle. A model for the membranolytic action of MLT and MLT-like peptides is proposed.

Although the cytolytic action of the bee venom peptide melittin (MLT)[1] has long been recognized (Sessa et al., 1969), the biophysical mechanisms underlying its membranolytic effects are still unclear. Three fundamentally distinct hypotheses have been proposed. One asserts a perturbation of the membrane bilayer in which the peptide acts as a sort of mechanical "wedge" between lipid molecules, resulting in

† This work was supported in part by PHS Grant GM34847 to F.G.P. and GM29864 to R.M.

* Address correspondence to these authors.
‡ Mayo Foundation.
§ Current address: Howard Hughes Medical Institute, University of Texas Southwestern Medical Center, Dallas, TX 75235-9050.
‖ Indiana University-Purdue University at Indianapolis (IUPUI).
⊥ Rutgers University.

[1] Abbreviations: ATF-FTIR, attenuated total reflectance-Fourier transform infrared; CD, circular dichroism; CMC, critical micelle concentration; CPMG, Carr-Purcell-Meiboom-Gill; CSA, chemical shift anisotropy; DMPC, dimyristoyl-L-α-phosphatidylcholine; LDAO, lauryldimethylamineoxide; MLPC, monolauroyl-L-α-phosphatidylcholine; MLT, melittin; MLT-W19, ([$^{13}C\delta_1$]L-Trp19,[$^{13}C\alpha$]Gly12)melittin; MLT-W17, ([$^{13}C\delta_1$]L-Trp17,[$^{13}C\alpha$]Gly12,Leu19)melittin; MLT-W11, ([$^{13}C\delta_1$]L-Trp11,[$^{13}C\alpha$]Gly12,Leu19)melittin; MLT-W9, ([$^{13}C\delta_1$]L-Trp9,[$^{13}C\alpha$]Gly12,Leu19)melittin; MMPC, monomyristoyl-L-α-phosphatidycholine; NMR, nuclear magnetic resonance; NOE, nuclear Overhauser effect; POPC, palmitoyloleoyl-L-α-phosphatidylcholine; Tris, tris(hydroxymethyl)aminomethane.

0006-2960/92/0431-1301$03.00/0

structural disruption of the opposed membrane leaflets (Dawson et al., 1978; Vogel et al., 1983). A second hypothesis maintains that MLT and related cytolytic peptides act by increasing the curvature of the bilayer so that its structural integrity is compromised (Batenburg & de Kruijff, 1988). A third hypothesis proposes that MLT is a pore-forming oligomer in lipid bilayers. Proponents of the latter model have demonstrated (i) that MLT acts as a concentration-dependent, nonselective, voltage-sensitive channel (Tosteson & Tosteson, 1981), (ii) that the kinetics of cytolysis show a $[MLT]^4$ concentration dependence (DeGrado et al., 1982), and (iii) that fluorescence energy transfer occurs between membrane-bound MLT monomers (Vogel & Jähnig, 1986). In contrast to the last hypothesis, the first two hypotheses do not require that lipid-bound MLT be oligomeric. Indeed, there are fluorescence (Hermetter & Lakowicz, 1986) and EPR data (Altenbach & Hubbell, 1988; Altenbach et al., 1989) which argue against the existence of MLT tetramers in lipid dispersions, at least at peptide concentrations which are sufficient to cause membrane disruption.

While much attention has focused on resolving MLT structure–function issues, the dynamics (i.e., motional rate constants and order parameters) of lipid-bound MLT have not yet been extensively investigated. John and Jähnig (1988), Vogel and Rigler (1987), and Georghiou et al. (1982) have all studied the dynamics of MLT–lipid complexes by analysis of tryptophan (Trp) fluorescence anisotropy decay. These data have been interpreted in terms of both local motion of the indole side chain (about χ_1 and χ_2 dihedral angles) and rotational motion of the entire peptide to explain complex anisotropy decays containing components with correlation times as short as 0.1 ns and as long as 20 ns. However, extrapolating from fluorescence anisotropy of the Trp side chain to obtain information relevant to peptide chain dynamics is difficult. A more direct analysis of peptide backbone mobility is needed. The question is significant because the rate and magnitude of peptide chain motion may well influence MLT function independent of the structure, per se, of the lipid-bound peptide (i.e., monomer versus oligomer).

To further probe the dependence of MLT function on peptide dynamics, we have sought to answer the following questions. Is a lipid-bound MLT oligomer necessary for its cytolytic action? Must MLT be helical to effect cytolysis? How does binding to lipids affect the dynamics of the MLT peptide chain and of a single Trp side chain placed at various positions in the sequence?

To examine these questions, synthetic "native" MLT and three analogues were prepared by solid-phase methods (Weaver et al., 1989a). Synthetic native MLT is denoted MLT-W19. A Trp residue was substituted for Leu9, Thr11, or Leu17 in the analogues MLT-W9, MLT-W11, and MLT-W17, respectively. The native Trp19 residue was replaced by leucine in each analogue. All four peptides were specifically labeled with ^{13}C (99%) at the $C\delta_1$ position of the single Trp residue and at the $C\alpha$ position of Gly12. Fluorescence, CD, attenuated total reflectance (ATR) FTIR, and NMR techniques were employed to determine the structural disposition of the peptides in lipid environments, and combined fluorescence and NMR data were used to study Trp dynamics. NMR alone was used to monitor the dynamics of the Gly12 α-carbon with the expectation that motion of this central Gly residue would characterize peptide chain dynamics, at least in its immediate vicinity. Previous work on the structure and dynamics of these peptides in aqueous lipid-free solutions indicated that none of the analogues form discrete soluble oligomers in solution, yet all retain cytolytic activity (Weaver et al., 1989a,b). We now present spectroscopic data relevant to the structure and dynamics of the lipid-bound MLT peptides. The results of these experiments, though obtained from spectroscopic techniques which vary widely in sensitivity and "structural" selectivity, are qualitatively, and essentially quantitatively, consistent. This information is used to develop a model for the membranolytic mechanism of MLT and the analogues.

Materials and Methods

MLT Peptides. Solid-phase synthesis and characterization of synthetic "native" melittin (MLT-W19) and analogues (MLT-W17, MLT-W11, and MLT-W9) have been described elsewhere (Weaver et al., 1989a).

CD Spectroscopy. Circular dichroism spectra of the synthetic peptides were obtained on a JASCO J-500A spectropolarimeter calibrated with (+)-10-camphorsulfonic acid. Samples were contained in 1-mm path length cylindrical cells maintained at 20 °C. Spectra were obtained as the average of eight scans taken from 260 to 180 nm at a scan rate of 20 nm min^{-1} with a sampling interval of 0.2 nm. Data were analyzed as described by Weaver et al. (1989a). CD spectra were obtained for each peptide as a function of MMPC concentration by titrating aqueous peptide (20 μM) with a concentrated (3.5 mM) MMPC solution also containing 20 μM peptide. Spectra were also obtained for each peptide in the presence of a fixed concentration of sonicated DMPC vesicles (1.09 mM) to which peptide was added to a final concentration of 20 μM. DMPC vesicles were prepared by sonication of ~8 mL of a lipid suspension for 15 min at 25 ± 2 °C. The sonicated solution was centrifuged at 2000 rpm for 10 min to remove titanium fragments from the sonicator tip. Vesicle suspensions were then allowed to anneal for 30 min at 30 °C before use. All solutions were buffered with 10 mM Tris, pH 7.5 (HCl).

ATR–FTIR Spectroscopy. The methods for sample preparation and acquisition of polarized ATR–FTIR spectra have been given elsewhere (Brauner et al., 1987). DPPC- and/or POPC–peptide films were chosen in preference to DMPC purely for technical reasons. At ambient relative humidity and temperature, these lipids exist in a partially ordered gel or liquid-crystalline state. As such, they are relatively stable even in the presence of lipid-destabilizing peptides. "Wet" films or bulk water studies have proven difficult because MLT tends to deplete the ATR crystal surface of the lipid to form soluble peptide–lipid micelles. Thus, comparisons of the ATR–FTIR results with the CD, fluorescence, and NMR data must be interpreted cautiously.

The complex contour observed for the amide I mode (1620–1695 cm^{-1}) of each peptide was decomposed using second-derivative spectroscopy and curve fitting. Band positions for final curve fitting were determined from second-derivative spectra. Estimates of the relative contributions of peak areas to the amide I contour were obtained from the results of curve fitting.

The orientation of peptide helical segments with respect to the bilayer plane, as estimated from the dichroic ratio R^{ATR}, is calculated from the relation

$$R^{ATR} = \frac{A_\parallel}{A_\perp} = \frac{E_x^2}{E_y^2} + \frac{E_z^2[f\cos^2\alpha + (1-f)/3]}{E_y^2[(f/2)\sin^2\alpha + (1-f)/3]} \quad (1)$$

where $A_\parallel$ and $A_\perp$ are the parallel and perpendicular IR absorption components; E_x, E_y, and E_z are the electric field components in the x, y, and z directions; $\alpha = 22°$ is the angle between the transition moment of the amide I vibration and

the helix axis (Nabedryk et al., 1982); and $f = (1/2)(3\langle\cos^2\theta_c\rangle - 1)$ is an orientational order parameter where θ_c is the average angle that the peptide c (helix) axis makes with the bilayer normal. For native MLT, a model consistent with the X-ray structure of MLT (Terwilliger & Eisenberg, 1982a,b) was invoked. In this model, the peptide is assumed to lie partially within the bilayer as a rigid bent α-helical rod (Brauner et al., 1987). For the current work, it is assumed that all of the MLT peptides adopt a fiber-type orientation wherein all azimuthal angles sampled by the peptide in the plane of the ATR crystal are equally probable (Fraser, 1953). The ATR crystal plane is taken to be equivalent to the bilayer plane. The electric field intensities were estimated from the Fresnel equations for thin films [cf. Harrick (1979) and Brauner et al. (1987)] to be $E_x = 1.41$, $E_y = 1.46$, and $E_z = 0.728$.

Fluorescence Spectroscopy. Emission spectra were obtained on a Perkin-Elmer MPF-66 fluorometer with an excitation wavelength of 280 nm (2-nm band-pass). Steady-state anisotropy measurements were made on an SLM-4800 fluorometer in the L-format with an excitation wavelength of 295 nm (1-nm band-pass). The emission was collected through a Schott WG-345 cut-on filter. Fluorescence lifetimes were measured using multifrequency phase modulation techniques as described previously (Weaver et al., 1989b). Titrations with MMPC were performed as described above for CD experiments in 0.005–1.0 mM MMPC and 5 μM peptide at 20 °C. Fluorescence emission spectra and steady-state fluorescence anisotropy measurements were obtained from the same samples. Steady-state anisotropy and emission spectra were also obtained for each of the peptides (5 μM) added to sonicated suspensions of DMPC vesicles (~1 mM) in the presence and absence of 1.2 M NaCl at 20 and 30 °C. Fluorescence lifetimes were measured at 25 °C for the peptides (15 μM) in buffer alone and in 1 mM MMPC and at 30 °C in the presence of 1 mM DMPC vesicles. All solutions were buffered with 10 mM Tris, pH 7.5 (HCl). DMPC vesicles were prepared as described above.

NMR Spectroscopy. ^{13}C NMR T_1, T_2, and steady-state NOE measurements were performed at 75.4 MHz on a Nicolet NT-300 FT spectrometer. Peptide samples (~2.5 mL) were placed in 12-mm tubes and maintained at 20 ± 1 °C. Approximately 5 μL of 1,4-dioxane was added to each sample as an internal ^{13}C chemical shift reference at 67.37 ppm (Shindo et al., 1978). All T_1 determinations employed a 180°–τ–90° inversion–recovery pulse sequence with a delay of $\geq 5T_1$. T_2 values were measured using a CPMG pulse sequence (Meiboom & Gill, 1958) with a composite 180° refocusing pulse to correct for field inhomogeneity and off-resonance diminution of field strength. Two- or three-parameter single-exponential fits were used in extracting T_1 and T_2 values from the data. Gated decoupling was used to measure the NOE, collecting alternate scans (with or without NOE) into adjacent memory blocks. A delay of $\geq 9T_1$ was used between observation pulses due to the nonexponential decay of this relaxation parameter. Broad-band noise decoupling of protons was used in all relaxation measurements. Relaxation data were typically collected as 8K data points with a spectral width of ±4505 Hz using quadrature phase detection.

Titration of peptide samples (0.9–1.5 mM in D_2O) with phospholipid was carried out by successive addition of aliquots of a concentrated MMPC solution (0.68 M) in D_2O. ^{13}C NMR spectra were obtained for each peptide in the presence of 0, 10, 30, and 60 mM MMPC, while relaxation data were obtained only for selected samples (see below). Unless noted otherwise, all samples were buffered with demetallized 10 mM Tris, pH 7.5, in D_2O. pH values are direct meter readings and are uncorrected for an isotope effect.

Analysis of Peptide Dynamics. Motional parameters characterizing Trp side chain and peptide backbone (Gly Cα) dynamics in peptide–micelle and peptide–vesicle complexes were calculated from observed steady-state fluorescence anisotropy, mean fluorescence lifetime, and/or ^{13}C NMR relaxation values. Details of the methodology have been given elsewhere (Weaver et al., 1989b). The principles underlying the analyses are summarized here only briefly.

(*1*) *Analysis of Fluorescence Data.* If, in the decay of fluorescence anisotropy $r(t)$ to zero, the overall correlation time of a macromolecule τ_m is independent of the effective correlation time τ_e for local or segmental motion of an attached fluorophore, then the following empirical expression for the time-dependent fluorescence anisotropy can be written:

$$r(t) = [(r_0 - r_\infty)e^{-t/\tau_e} + r_\infty]e^{-t/\tau_m} \quad (2)$$

The term r_0 gives the fundamental anisotropy of the fluorophore which is a function of the relative orientation of the absorption and emission transition dipoles at a given excitation wavelength, and r_∞ is the limiting hindered anisotropy (Kinosita et al., 1977). If the quantities r_0 and r_∞ are related to an orientational order parameter, $S = (r_\infty/r_0)^{1/2}$, then, assuming the fluorescence decay to be a single exponential[2] with lifetime τ_f, the steady-state anisotropy $\bar{r}$ can be written

$$\bar{r} = r_0\left[\frac{1 - S^2}{1 + \tau_f(\tau_e^{-1} + \tau_m^{-1}) + S^2(1 + \tau_f/\tau_m)^{-1}}\right] \quad (3)$$

A set of S and τ_e values can be derived from fluorescence lifetime and steady-state anisotropy data alone from eq 3, provided that one has a reliable value for the overall correlation time of the macromolecule (or, e.g., a peptide–lipid complex). Further, one must also have a reasonably accurate r_0 value appropriate to the excitation wavelength used in steady-state anisotropy and lifetime determinations. An r_0 of 0.26 at 294 nm for tryptophan in water at pH 7.0 (Ruggiero et al., 1990) was used in calculating Trp side chain motional parameters from fluorescence or combined fluorescence and NMR data.

(*2*) *Analysis of NMR Data.* Information about motion of ^{13}C nuclei is contained in the relaxation rates T_1^{-1} and T_2^{-1} as well as in the steady-state NOE. If the magnetic dipole–dipole interaction of the ^{13}C nucleus with its directly bonded proton or protons and chemical shift anisotropy (CSA) are taken to dominate these quantities [for further discussion, see Weaver et al. (1989b)], they can be written[3]

$$T_1^{-1} = \frac{n\hbar^2\gamma_C^2\gamma_H^2}{4r_{CH}^6}[J(\omega_H - \omega_C) + 3J(\omega_C) + 6J(\omega_H + \omega_C)] + (\Delta\delta)^2\omega_C^2J(\omega_C) \quad (4)$$

$$T_2^{-1} = \frac{n\hbar^2\gamma_C^2\gamma_H^2}{8r_{CH}^6}[4J(0) + J(\omega_H - \omega_C) + 3J(\omega_C) + 6J(\omega_H + \omega_C) + 6J(\omega_H)] + (1/6)(\Delta\delta)^2\omega_C^2[4J(0) + 3J(\omega_C)] \quad (5)$$

$$\mathrm{NOE} = 1 + \frac{\gamma_H}{\gamma_C}[[6J(\omega_H + \omega_C) - J(\omega_H - \omega_C)]/[J(\omega_H - \omega_C) + 3J(\omega_C) + 6J(\omega_C + \omega_H) + (4r_{CH}^6/n\hbar^2\gamma_C^2\gamma_H^2)(\Delta\delta)^2\omega_C^2J(\omega_C)]] \quad (6)$$

[2] Although eq 3 can be modified to accept multiexponential fluorescence lifetime data, we find that for the large τ_m values characteristic of micelles, S and τ_e change <0.1% from their values calculated using the mean fluoresence lifetime, $\tau_f = \sum_i\alpha_i\tau_i^2/\sum_i\alpha_i\tau_i$.

In these expressions, n is the number of protons directly bonded to the ^{13}C nucleus, $\hbar$ is Planck's constant divided by 2π, γ_C and γ_H are the magnetogyric ratios for ^{13}C and ^{1}H, ω_C and ω_H are the ^{13}C and ^{1}H resonance frequencies, r_{CH} is the ^{13}C–H bond distance, and $J(\omega)$ is the spectral density. These relations assume that the chemical shift tensor, δ, is axially symmetric about the $^{13}C\delta_1$–H bond vector such that $\Delta\delta = \delta_\parallel - \delta_\perp$. Direct measurements of tensor principal values for $^{13}C\delta_1$–Trp, however, have indicated that the chemical shift tensor is not axially symmetric (B. A. Cornell, personal communication). To account for this quantitatively, $\Delta\delta$ can be written

$$\Delta\delta = \frac{3}{2}\delta_{zz}\left(1 + \frac{\eta^2}{3}\right)^{1/2} \quad (7)$$

where $\eta = |(\delta_{yy} - \delta_{xx})/\delta_{zz}|$ is a tensor asymmetry parameter (Abragam, 1961) and $(\delta_{xx}, \delta_{yy}, \delta_{zz})$ are elements of the traceless chemical shift tensor. By this method, we calculate $\Delta\delta = 137.5$ ppm for $^{13}C\delta_1$–Trp and have used this value in the analyses below. Chemical shift tensor principal values have also been reported for the Cα of glycine by Haberkorn et al. (1981); eq 7 yields $\Delta\delta = 33.8$ ppm, which is used in the analyses below. The value for r_{CH} is taken to be 1.09 Å for the Trp $C\delta_1$–H bond distance and 1.11 Å for the mean Gly Cα–H bond distance (Dill & Allerhand, 1979).

The spectral density proposed by Lipari and Szabo (1982a)

$$J(\omega) = \frac{2}{5}\left[\frac{S^2\tau_m}{1 + \omega^2\tau_m^2} + \frac{(1 - S^2)\tau}{1 + \omega^2\tau^2}\right] \quad (8)$$

where $\tau^{-1} = \tau_e^{-1} + \tau_m^{-1}$, is used in the preceding expressions for T_1^{-1}, T_2^{-1}, and NOE. In this so-called "model-free" approach, S is a "generalized order parameter" for local motion of a given ^{13}C–H vector and τ_e and τ_m are as defined above. The spectral density is derived from an autocorrelation function for the ^{13}C–H vector assuming, as in the fluorescence expressions, that overall molecular motion is isotropic and that the internal and overall motions are independent. So, provided that the indole ring is rigid, the motion of its ^{13}C–H vector should reflect motion of the Trp side chain as a whole. Similarly, the motion of the mean $^{13}C\alpha$–H bond vector of glycine should be indicative of the flexibility of the peptide chain in the vicinity of the labeled residue.

Given a set of T_1, T_2, and NOE data, the motional variables S, τ_e, and τ_m can be derived by evaluating the nonlinear system defined by eqs 4–8. A unique solution, if it exists, requires the measurement of three or more independent relaxation values, i.e., T_1, T_2, and NOE at a single spectrometer frequency, or other combinations at more than one frequency. When fewer than three relaxation values are known, constraints on S, τ_e, and τ_m can be established from the available data. For example, if T_1 and NOE data are available, the spectral density can be systematically evaluated over all "physically reasonable" τ_m values; S and τ_e are adjusted at each τ_m until the calculated and observed relaxation values agree. Results can then be presented in the form of plots of S or τ_e as a function of τ_m. In this example, such plots would be referred to as T_1–NOE curves. In general, one can generate S versus τ_m or τ_e versus τ_m plots given values for any two NMR relaxation parameters, the remaining possibilities being T_2–NOE and T_1–T_2 curves. In the peptide–micelle systems studied, measured T_2 values were exceeding small (≤9 ms) and therefore were difficult to measure accurately or with acceptable precision. Hence, in analyses of NMR relaxation data below, only T_1–NOE curves are presented for the micelle-bound MLT peptides.

(3) Analysis of Combined Fluorescence and NMR Data. Equations 3–8 imply a relationship between fluorescence and NMR observables. Under appropriate experimental conditions and theoretical assumptions [for a discussion, see Weaver et al. (1989b)], these expressions allow data from the two techniques to be combined to obtain values for motional parameters descriptive of Trp side chain dynamics. This approach has been taken in analyses of combined fluorescence and NMR data presented below. Specifically, measured steady-state fluorescence anisotropy and fluorescence lifetime values were substituted for NMR spin–spin relaxation times because of inaccuracies inherent in measurements of very short T_2's characteristic of the micelle-bound peptides. In analogy with the NMR data analysis methods discussed above, steady-state fluorescence anisotropy and fluorescence lifetime data are used with NMR T_1 and NOE data to generate two-parameter $T_1 - \bar{\tau}$ and NOE $- \bar{\tau}$ curves for the MLT peptide–micelle complexes. The common intersection (if it exists) of such curves provides a "unique" solution for the motional variables describing the dynamics of the Trp side chain.

(4) Physical Interpretation of Order Parameter Values. The indole moiety of the Trp side chain can rotate about α–β (χ_1) and β–γ (χ_2) bonds. If one assumes that the planar ring moves only about the β–γ bond and that any angle is equally probable in range of $\pm\phi_0$ about an equilibrium orientation, then the square of the order parameter can be expressed explicitly as

$$S^2 = \frac{1}{4}(3\cos^2\theta_0 - 1)^2 + 3\left[\sin\theta_0\cos\theta_0\left(\frac{\sin\phi_0}{\phi_0}\right)\right]^2 + \frac{3}{16}\left[\sin^2\theta_0\left[\frac{\sin(2\phi_0)}{\phi_0}\right]\right]^2 \quad (9)$$

where $\theta_0 = 72.5°$ is the fixed angle between the $C\delta_1$–H vector and the β–γ bond. Equation 9 is used to calculate ϕ_0 values corresponding to experimentally determined order parameters [for further discussion, see Weaver et al. (1989b)].

Results and Discussion

Structure of the Lipid-Bound Peptides

(1) CD Studies. CD experiments have generally yielded $-[\theta]_{222}$ values of 10 000–30 000 deg cm^2 dmol^{-1} for naturally occurring MLT in the presence of a wide variety of detergent micelles and liposomal (bilayer) suspensions (Dawson et al., 1978; Drake & Hider, 1979; Lauterwein et al., 1979; Knoppel et al., 1979; Strom et al., 1982; Yunes, 1982; Chandani & Balasubramanian, 1986; Kubota & Yang, 1986). The data presented in Table I for MLT-W19 in MMPC micelles and DMPC vesicles support published observations. MLT-W19 shows an essentially linear increase in α-helix content with MMPC concentration, attaining ~73% α-helix in 1 mM MMPC. By contrast, the helicity of MLT-W11 is significantly greater (91%), while MLT-W9 and MLT-W17 show less helix content (62% and 59%, respectively) under identical conditions. In DMPC vesicles, trends observed in the micellar system recur, although peptide fractional helicities are clearly less than in the peptide–micelle complexes. The α-helix content of MLT-W19 and MLT-W11 (56% and 52%, respectively) is essentially twice that observed for MLT-W9 and MLT-W17 (both 28%).

From these results, one can infer that the *relative* helix-forming potential of the MLT peptides is independent of the

[3] The T_2^{-1} expression given as eq 8 in Weaver et al. (1989b) contains a typographical error in the inclusion of an additional factor $J(\omega_C)$ in the CSA term.

Table I: CD Parameters for MLT Peptide–Lipid Complexes[a]

	MLT-W19		MLT-W17		MLT-W11		MLT-W9	
lipid (mM)	$-[\theta]_{222}$	α-helix (%)	$-[\theta]_{222}$	α-helix (%)	$-[\theta]_{222}$	α-helix (%)	$-[\theta]_{222}$	α-helix (%)
MMPC								
0.05 mM	2154	1	1952	0	3673	6	1635	−1
0.10 mM	4067	7	2663	2	5154	11	3087	4
0.20 mM	7692	20	4750	10	8712	24	6346	15
0.50 mM	16144	50	10683	31	17894	56	13692	41
1.00 mM	22577	73	18673	59	27865	91	19452	62
DMPC								
1.09 mM	17904	56	10077	28	16837	52	9798	28

[a] Mean residue ellipticity is expressed in deg cm^2 dmol^{-1}. The fractional helicity was determined using $[\theta]_{222}$ values of −2000 and −28 400 deg cm^2 dmol^{-1} for 0% and 100% α-helix, respectively (Kubota & Yang, 1986).

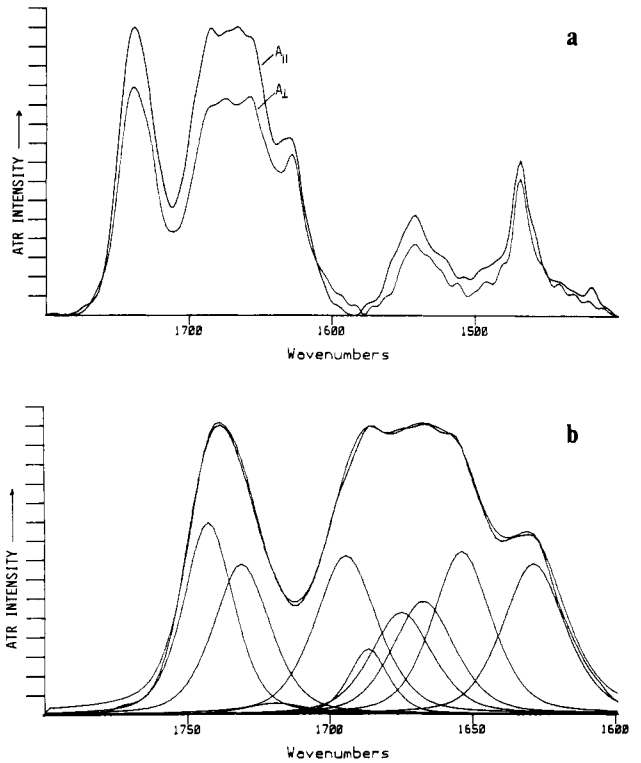

FIGURE 1: Typical ATR–FTIR spectra for MLT and MLT analogues bound to diacylphospholipid films. (a) Parallel and perpendicular spectral components of MLT-W9/DPPC on a germanium substrate with an incident angle of 45°. (b) Results characteristic of the curve fitting algorithm. The data shown are for the parallel component of MLT-W9/DPPC. The peak positions for the various subbands are determined from second-derivative spectroscopy.

lipid substrate and is thus an intrinsic property of the peptide, while the *absolute* helix content taken by a given peptide is modulated by the lipid environment. DMPC, even in the fluid (L_α) phase, is apparently less able to induce a helical conformation in these peptides than its lysolipid, MMPC. Similar behavior has been observed for other helix-forming peptides in the presence of bilayer- versus micelle-forming lipids, e.g., LamB signal sequences (McKnight et al., 1989).

(*2*) *ATR–FTIR Studies.* Polarized ATR–FTIR measurements provide (i) an estimate of peptide secondary structure, (ii) a semiquantitative measure of the static orientational distribution of α-helical secondary structure with respect to the bilayer plane, and (iii) a qualitative indication of the phospholipid acyl chain configurational state [for a discussion, see Brauner et al. (1987)].

A polarized ATR–FTIR spectrum typical of MLT peptide–DPPC films and results characteristic of the band-fitting procedure referred to above are shown in Figure 1. The spectral region plotted includes the amide I mode (1620–1690 cm^{-1}) of the peptide bond and the phospholipid C=O stretching vibration (1700–1750 cm^{-1}). Correlations of spectral data with secondary structure for the amide I mode have been detailed elsewhere (Mendelsohn & Mantsch, 1986; Byler & Susi, 1986).

Table II: Polarized ATR–FTIR Parameters for MLT Peptide–Lipid Complexes[a]

sample	R^{ATR}	α-helix (%)	f	$\nu^{sym}_{CH_2}$ (cm^{-1})	$\Delta\nu^{sym}_{CH_2}$ (cm^{-1})[b]
MLT-W19					
DPPC	1.46	49	0.34	2850.8	0.4
POPC	nd[c]			2853.9	2.5
MLT-W17					
DPPC	1.50	30	0.38	2851.6	1.2
POPC	1.47	28	0.35	2854.2	2.8
MLT-W11					
DPPC	1.64	23	0.48	2851.1	0.7
POPC	1.64	26	0.48	2854.3	2.9
MLT-W9					
DPPC	1.30	18	0.17	2851.5	1.1
POPC	nd			nd	

[a] Peptide fractional helicity is determined from the fractional contribution to the amide I band of the spectral component near 1656–1657 cm^{-1}. Amide I band dichroic ratios, R^{ATR}, are related to an orientational order parameter, f, by eq 1. [b] This parameter measures the increase in the CH_2 symmetric stretching frequency from the baseline values of 2850.4 cm^{-1} for DPPC and 2851.4 cm^{-1} for POPC under the experimental conditions used (for further discussion, see text). [c] Not determined.

The α-helix amide I band occurs at 1656–1657 cm^{-1} for all four MLT peptides. The assumption generally made for quantitative analysis (Surewicz et al., 1987) is that IR molar extinction coefficients are the same for all secondary structural elements. Under this hypothesis, the fractional area of the amide I contour occupied by the 1656–1657-cm^{-1} band, as determined by the curve fitting process, converts directly to fractional helicity values given in Table II. MLT-W19 contains 49% α-helix in DPPC films as monitored by the ATR–FTIR measurements. This result is in good accord with the CD data presented above for MLT-W19 bound to DMPC vesicles (56%). Substantially lower α-helical content is noted for MLT-W9 and MLT-W17 (18% and 30%, respectively), which is also in reasonable agreement with the CD data (both 28%). The main difference between the ATR–FTIR and CD data is that the former show substantially less α-helix for MLT-W11 (23% versus 52%). A possible explanation for this disparity arises from consideration of the peptide–DMPC fluorescence data. Specifically, the magnitude of the Trp fluorescence blue-shift, especially for MLT-W11, was found to depend strongly on the degree to which peptide–vesicle binding occurred. The latter is promoted by high ionic strength or high lipid to peptide ratios (see fluorescence results below). For technical reasons (see Materials and Methods above), neither of these conditions was maintained in the ATR–FTIR

Table III: ^{13}C NMR Data, Steady-State Fluorescence Anisotropy and Mean Fluorescence Lifetime Data, and Calculated Motional Parameters for Aqueous MLT Peptides and MLT Peptide–Lipid Complexes[a]

sample	δ (ppm)	$\Delta\nu_{1/2}$ (Hz)	T_1 (s)	NOE	$\bar{r}$	τ_f (ns)	S	τ_e (ns)	τ_m (ns)
MLT-W19 (monomer)									
W19 Cδ_1	125.1	6.4	0.182	1.78	0.039	2.75	0.64	0.124	1.24
G12 Cα	43.0	10.3	0.101	2.06			0.61	0.247	(1.24)[b]
MLT-W19 (tetramer)									
W19 Cδ_1	125.1	17.3	0.271	1.27	0.100	2.17	0.73	0.026	5.43
G12 Cα	44.8	21.1	0.168	1.28			~1	–	(5.43)
MLT-W19/MMPC									
W19 Cδ_1	125.1	32.7	0.435	1.52	0.124	1.59	0.73	0.049	11.5
G12 Cα	44.6	67.7	0.227	(1.10)[c]			id[d]	id	id
MLT-W17/MMPC									
W17 Cδ_1	125.3	24.2	0.402	1.35	0.117	3.39	0.77	0.034	10.4
G12 Cα	44.7[e]	62.9	0.299	1.45			0.72	0.029	(10.4)
MLT-W11/MMPC									
W11 Cδ_1	126.0	33.4	0.442	1.44	0.123	2.06	0.74	0.040	11.4
G12 Cα	45.4	60.9	0.310	1.37			0.76	0.023	(11.4)
MLT-W9/MMPC									
W9 Cδ_1	124.4	18.6	0.323	(1.02)	0.128	2.90	0.77	0.123	(11.4)
G12 Cα	44.4	42.0	0.346	(1.12)			id	id	id

[a] NMR data were obtained at a lipid to peptide ratios of ~59 (MLT-W19), ~57 (MLT-W17), ~24 (MLT-W11), and ~32 (MLT-W9). Fluorescence data were collected at a lipid to peptide ratio of ~67. [b] Overall correlation times given in parentheses indicate that this quantity was held constant in calculating the corresponding S and τ_e values. [c] NOE values given in parentheses indicate that the observed value was less than the theoretical minimum NOE (see text). [d] Insufficient data for calculation of motional parameters. [e] A small additional peak corresponding to free MLT-W17 monomer was observed concomitantly at 43.3 ppm (see text).

experiments. Still, considering the rather extreme variation in sample preparation in the ATR–FTIR compared with the CD studies, the general agreement is remarkable.

The ATR–FTIR polarization ratios for the α-helix bands and associated orientational order parameters are compiled in Table II. The data reveal the highest degree of helical segment orientational order for MLT-W11, intermediate and essentially equal orientational order for MLT-W17 and MLT-W19, but nearly random orientational order for MLT-W9. A completely random orientation ($f = 0$, $\theta_c = 54.7°$) would yield an $R^{ATR} = 1.18$, so the observed value of 1.30 for MLT–W9 is indicative of relatively poor orientational order.

Data are also included in Table II for symmetric CH_2 stretching frequencies and changes in these frequencies which have been used extensively to probe configurational order and phase transitions in phospholipids. In general, CH_2 stretching frequencies increase during processes which induce acyl chain trans–gauche isomerization. Frequency increases are small (1–4 cm^{-1}) during lipid melting events, but since this parameter can be monitored with a precision of better than 0.05 cm^{-1}, it becomes a useful structural probe (Snyder et al., 1982). Although the frequency increase is not a linear function of gauche rotamer formation, qualitative aspects of a peptide's influence on lipid organization may be deduced. The data in Table II show that the MLT analogues induce a larger increase in the DPPC stretching band frequency than does MLT-W19. Interestingly, MLT-W11, MLT-W17, and MLT-W19 *all* induce a substantial disordering of the POPC system. The latter result is remarkable since POPC is in a liquid-crystalline state under the experimental conditions and would not be expected to show significantly more disorder in the presence of peptide than exists naturally in this state.

(3) Fluorescence Studies. Titrations with synthetic MMPC were carried out for each of the MLT peptides in the presence and absence of 1.2 M NaCl. The presence of NaCl did not affect the *relative* changes observed in fluorescence emission maxima (λ_{max}), intensity ratios (I/I_0), and steady-state anisotropy ($\bar{r}$) values as a function of MMPC content, but it did shift each titration curve so that corresponding changes occurred at lower lipid concentrations in the presence of NaCl. In Figure 2, plateau values for λ_{max}, I/I_0, and $\bar{r}$ occur at ~0.2 mM MMPC in the absence of NaCl. No further changes in

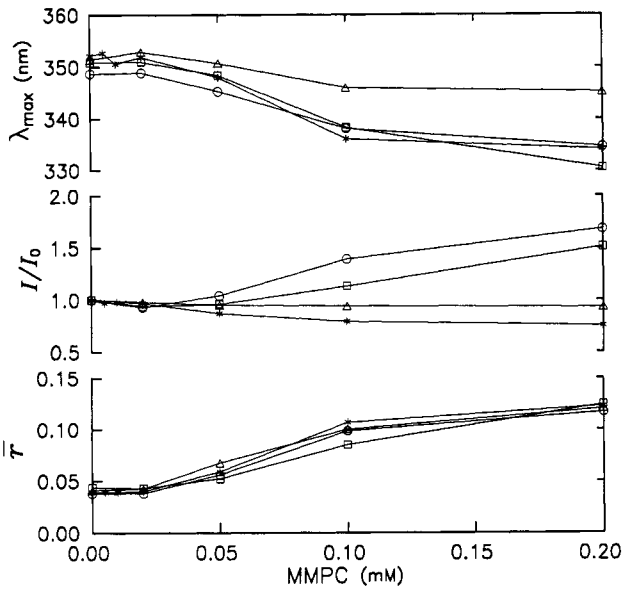

FIGURE 2: Fluorescence emission maximum (λ_{max}), normalized fluorescence intensity ratio at λ_{max} (I/I_0), and steady-state fluorescence anisotropy ($\bar{r}$) for MLT peptides as a function of MMPC concentration. MLT-W19 (*), MLT-W17 (○), MLT-W11 (△), and MLT-W9 (□).

the fluorescence parameters were observed at higher lipid concentrations (up to 1 mM). Almost exactly the same endpoints were attained at ~0.1 mM MMPC in 1.2 M NaCl (data not shown). This observation almost certainly reflects a decrease in the CMC of the lysophospholipid at high salt concentrations (Tanford, 1981). The CMC of MMPC in pure water is 0.07 mM (Stafford et al., 1989). Noting an inverse relation between Trp fluorescence intensity and the apparent CMC of various phospholipids, Talbot et al. (1982) suggested that an "organized lipid substrate" promotes the interaction of MLT with phospholipids. The fluorescence data for the MLT analogues support this contention. When combined with NMR relaxation data to evaluate Trp side chain dyanmics, fluorescence data obtained at a lipid to peptide mole ratio of ~67 were used (see Table III). This value is comparable to that used in the NMR experiments and is greater than the lipid to peptide ratio above which no further changes occur

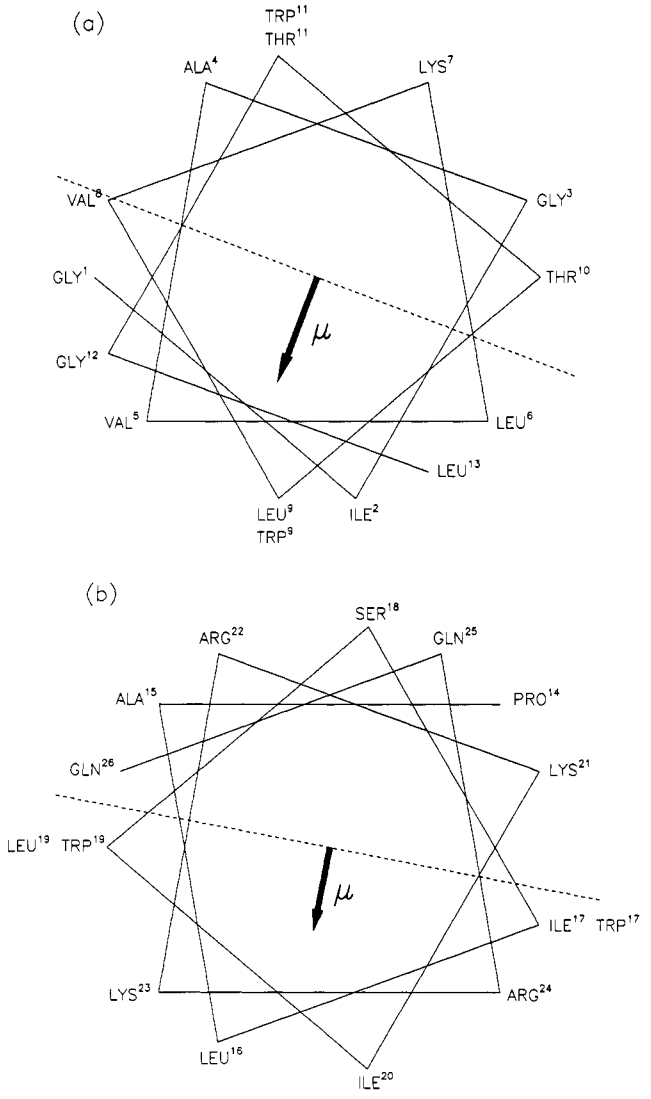

FIGURE 3: Helical wheel projections and calculated hydrophobic moments (μ) of MLT peptides. The dashed line indicates the lipid–water interface or boundary between hydrophobic and hydrophilic peptide surfaces predicted by the orientation of μ. Moments calculated for the MLT-W19 sequence vary by <15% in magnitude and <10° in direction among the MLT analogues. The innermost residues correspond to the MLT-W19 sequence; amino acid substitutions introduced in the various MLT analogues are shown peripherally. (a) Residues 1–13, $|\mu| = 3.34$. (b) Residues 14–26, $|\mu| = 2.51$.

in the fluorescence parameters (i.e., >0.2 mM MMPC $\approx$ 40 lipid/peptide).

The emission maximum of the MLT peptides shows the following trend: MLT-W9 < MLT-W19 $\leq$ MLT-W17 $\ll$ MLT-W11. This result is readily explained by examination of helical wheel projections (Schiffer & Edmundson, 1967) and hydrophobic moments (Eisenberg et al., 1984) shown in Figure 3 for these amphiphilic peptides. The design of the MLT analogues was, in fact, based on such considerations (Weaver et al., 1989a). The hydrophobic moment calculated for the amino-terminal 13 residues of MLT-W9 places its Trp residue almost precisely in the center of the hydrophobic face of the helix. By contrast, the Trp side chain of MLT-W11 is located almost diametrically on the opposing hydrophilic face of the helical peptide. A similar depiction of the 13 C-terminal residues of MLT-W19 and MLT-W17 again places the respective Trp side chains diametrically, yet both are quite close to the hydrophobic–hydrophilic boundary.

Given this result, it is very interesting that the fluorescence intensity ratios for the peptides (Figure 2) do *not* correlate with their respective blue-shifts. I/I_0 increases in the sequence: MLT-W19 < MLT-W11 $\ll$ MLT-W9 < MLT-W17. Moreover, $I/I_0 < 1$ for both MLT-W19 and MLT-W11, while it is between 1.5 and 2.0 for MLT-W9 and MLT-W17. Helical wheel projections (Figure 3) reveal that a helical conformation for MLT-W19 and MLT-W11 permits steric contacts between the indole side chain and Nϵ amino groups of Lys23 and Lys7, respectively. In these peptides, fluorescence of the Trp residue at position i might therefore be susceptible to intramolecular quenching by a Lys side chain at position $i \pm 4$ (Tanaka & Mataga, 1987). This explanation immediately raises the following question: Why is MLT-W17 fluorescence not also (intramolecularly) quenched by Lys21? One possible reason is that Lys21 is *not* protonated under the experimental conditions (pH 7.5). The following experimental observations support such a contention: (1) only protonated, positively charged Nϵ amino groups are efficient quenchers of Trp fluorescence (Tanaka & Mataga, 1987); (2) Quay and Tronson (1983) have determined pK_a values of 6.5 and 8.6 for Lys21 and Lys23, respectively, based on reactivity of monomeric MLT with 2,4,6-trinitrobenzenesulfonate; (3) the Lys21 amide proton exchange rate for micelle-bound MLT is "extremely slow" (>2 days) (Inagaki et al., 1989), suggesting that this residue (and side chain) is buried in the micelle interior; such a state would be energetically unfavorable for a charged Lys21 residue. We concede, however, that the lack of intramolecular quenching of MLT-W17 Trp fluorescence could also be explained by segmental nonhelicity of peptide residues near the Trp17 chromophore since CD experiments reported only 59% helicity for the MMPC-bound peptide.

The nearly uniform steady-state fluorescence anisotropy values (Figure 2) for the micelle-bound peptides attest to similar steric constraints to Trp side chain motion in all of the lipid–peptide complexes (see below). Talbot et al. (1982) have obtained similar results for MLPC titration of MLT.

In contrast to the MMPC studies, peptide fluorescence parameters depended on both temperature and salt concentration in MLT peptide–DMPC vesicle preparations. In the absence of added NaCl, λ_{max} values for all of the peptides uniformly shifted to longer wavelengths with increasing peptide concentration; specific values, however, depended on the type of phospholipid used and sample temperature (data not shown). However, λ_{max} was essentially independent of peptide concentration and temperature in the presence of 1.2 M NaCl. In this case, emission maxima showed a clear pattern: MLT-W9 (331 nm) < MLT-W19 (335 nm) $\simeq$ MLT-W17 (336 nm) < MLT-W11 (338 nm). The correspondence with the MMPC results is clear. One can infer that high salt concentration in some fashion stabilizes the lipid–peptide complexes. Since binding of MLT is presumed to depend, at least initially, on electrostatic interactions between positively charged peptide C-terminal residues and negatively charged phospholipid head groups, the presence of 1.2 M NaCl would not only diminish electrostatic effects but would also promote hydrophobic interactions. In the absence of salt, the uniform increase in λ_{max} with peptide concentration can be attributed to unfavorable lipid–peptide electrostatic interactions in a low ionic strength environment.

(*4*) *NMR Studies.* Chemical shift and line width data are compiled in Table III for the Trp $^{13}C\delta_1$ and Gly12 $^{13}C\alpha$ resonances of the MLT peptides in the presence of MMPC. The most striking effect observed upon addition of lysophospholipid to the respective peptides was noted for MLT-W9. Titration of a 0.98 mM MLT-W9 sample to 10 mM MMPC resulted in the appearance of relatively sharp peptide

^{13}C resonances, while *no* signals were detectable prior to addition of lipid. Addition of phospholipid clearly promotes the disaggregation of aqueous MLT-W9 and, by implication, very likely dissociates soluble, tetrameric native MLT as well. Dissociation of the aqueous MLT tetramer into peptide monomers upon interaction with micellar phospholipids was also proposed by Brown (1979), who observed essentially identical ^1H NMR spectra on titration of either monomeric or tetrameric native MLT with MLPC or LDAO.

Line widths for Trp $^{13}C\delta_1$ and Gly12 $^{13}C\alpha$ resonances (Table III) are consistent with partitioning of the respective peptides into the micellar structure such that the overall rotational diffusion of the peptide backbone reflects that of the mixed micelle. This observation is borne out quantitatively by relaxation measurements described below.

Chemical shift values for Gly12 $^{13}C\alpha$ of micelle-bound MLT-W9, MLT-W17, and MLT-W19 (44.5–44.7 ppm) coincide closely with that reported previously for aqueous MLT-W19 tetramer (44.7 ppm) (Weaver et al., 1989a). These chemical shifts represent a 1.5–1.7 ppm downfield shift of this resonance relative to that observed for the aqueous peptide monomers (43.0 ppm). Interestingly, an even greater downfield shift is observed for micelle-bound MLT-W11 (2.2–2.4 ppm). The downfield shift has been attributed to hydrogen-bond formation between the Gly12 amide group and the carbonyl group of Val8 accompanying α-helix formation (Weaver et al., 1989a). In that paper, it was proposed that tetramer formation by MLT-W19 contributes to the downfield shift only insofar as it stabilizes the α-helical conformation of MLT in aqueous solution; peptide oligomerization per se is *not* responsible for the phenomenon. This conclusion has been validated in a subsequent study in which *monomeric* MLT-W19 was titrated with 0–100% methanol. A progressive downfield shift from 43.0 to 44.6 ppm was observed for the Gly12 $^{13}C\alpha$ resonance coincident with increasing solvent-induced peptide α-helix content (Weaver et al., unpublished results). A comparable downfield shift of the Gly12 $^{13}C\alpha$ resonance is now observed for *all* of the MLT peptides in a micellar environment. These data thus support an α-helical conformation, at least for peptide residues 8–12, in the mixed peptide–lipid micelles. Further, the magnitude of the downfield shift appears to be correlated with the stability or extent of α-helix formation in the respective peptides. Specifically, CD data showed that the helix-forming potential of MLT-W11 is significantly greater than that of the other MLT peptides; the downfield shift of its Gly12 $^{13}C\alpha$ resonance is also significantly larger.

In distinction to the other MLT peptides, the Gly12 $^{13}C\alpha$ resonance of MLT-W17 in 10 mM MMPC (lipid/peptide, 9:1) was split into two peaks of approximately equal intensity centered at 44.7 and 43.0 ppm. In samples containing 30 or 60 mM MMPC, the downfield peak predominated, while the upfield peak was just barely detectable (data not shown). These peaks are assigned to the α-helical micelle-bound peptide and unstructured aqueous monomer, respectively. The coexistence of two peaks demonstrates that the free and micelle-bound MLT-W17 are in slow exchange. A similar slow-exchange phenomenon was previously observed for MLT-W19 monomer and tetramer in aqueous solution (Weaver et al., 1989a). Apparently, MLT-W17 has a lower affinity for the micellar environment compared with the other MLT peptides. This is noteworthy in light of CD data which showed that MLT-W17 also has the least helix-forming tendency among the MLT peptides. Thus, the ability to form an α-helix (not necessarily amphiphilic) is an intrinsic property dictated by the peptide sequence which does appear to correlate with the ability to initially bind to (but not disrupt) phospholipid substrates.

Chemical shift data for the Trp $^{13}C\delta_1$ resonance also appear to provide information about the relative solvent exposure of the Trp side chain in the MLT peptides. The change in the Trp $^{13}C\delta_1$ chemical shift on assuming a micelle-bound state, $d\delta = \delta_{lipid} - \delta_{water}$, did not vary with lipid concentration for any of the MLT peptides. The following values are therefore average changes measured in the presence of 10, 30, and 60 mM MMPC: MLT-W19, 0.0 ppm; MLT-W17, +0.3 ppm; MLT-W11, +0.7 ppm; MLT-W9, −0.9 ppm. A progressive upfield shift from 125.1 to 124.2 ppm has been observed for the Trp $^{13}C\delta_1$ resonance of MLT-W19 in methanol–water mixtures with increasing methanol content 0% to 100% (Weaver et al., unpublished results). The pronounced upfield shift of the MLT-W9 resonance is therefore consistent with partitioning of the Trp side chain into the relatively less polar micellar acyl chain environment which is thought to resemble bulk methanol in terms of dielectric permittivity and effect on peptide conformation (Gierasch et al., 1982). Further, the MLT-W11 Trp resonance demonstrates an opposite, downfield, shift nearly equal in magnitude to the upfield shift of MLT-W9. We believe this reflects a corresponding *increase* in the polarity of the Trp11 side chain environment due to increased accessibility to bulk solvent or close proximity of the indole ring to zwitterionic phospholipid head groups. The small downfield shift of the MLT-W17 Trp resonance might indicate a slight increment in polarity of the Trp17 environment, while the absence of a shift for MLT-W19 implies little or no change in the environment of the Trp19 side chain in water versus the micelle-bound state. The chemical shift (δ, not $d\delta$) of the Trp $^{13}C\delta_1$ resonance is directly correlated with the Trp fluorescence emission maximum in the presence of MMPC (i.e., MLT-W11 > MLT-W17 ≥ MLT-W19 > MLT-W9) even though all of the peptides demonstrate a blue-shifted λ_{max} relative to the spectra of the peptide monomers in water. We speculate that while the fluorescence experiments report a variable displacement of the entire *indole ring* (specifically, of its emission dipole) toward the apolar lipid chains, the Trp $^{13}C\delta_1$ *atom* is a much smaller position-sensitive probe which experiences a positive shift ($d\delta$) when close to charged phospholipid head groups and a negative shift when shielded by the apolar lipid side chains. Helical projections and hydrophobic moments shown in Figure 3 provide a structural model consistent with the experimental observations.

Considered as a whole, the CD, ATR–FTIR, fluorescence, and ^{13}C NMR data can be interpreted to give a remarkably consistent *structural* picture of MLT peptide–lipid interactions. As noted above, the isolated disparity in helix content found for the MLT-W11/DPPC system in the ATR–FTIR experiments can be explained by reduced lipid binding under the chosen experimental conditions. The spectroscopic results as they pertain to lipid-bound MLT peptide structure can be summarized in the following statements; (1) all of the MLT peptides bind as amphiphilic helices to phospholipid substrates; (2) MLT-W11 shows the greatest helix-forming propensity on binding to lipid substrates, it possesses the greatest degree of perpendicular orientational order with respect to the plane of the lipid bilayer, and its Trp side chain resides in the most polar environment—probably exposed to bulk solvent or lipid head groups; (3) MLT-W9, by contrast, shows relatively poor helix-forming ability in the presence of lipid substrates, it manifests essentially random orientational order with respect to the bilayer plane, and its Trp side chain sits in a relatively

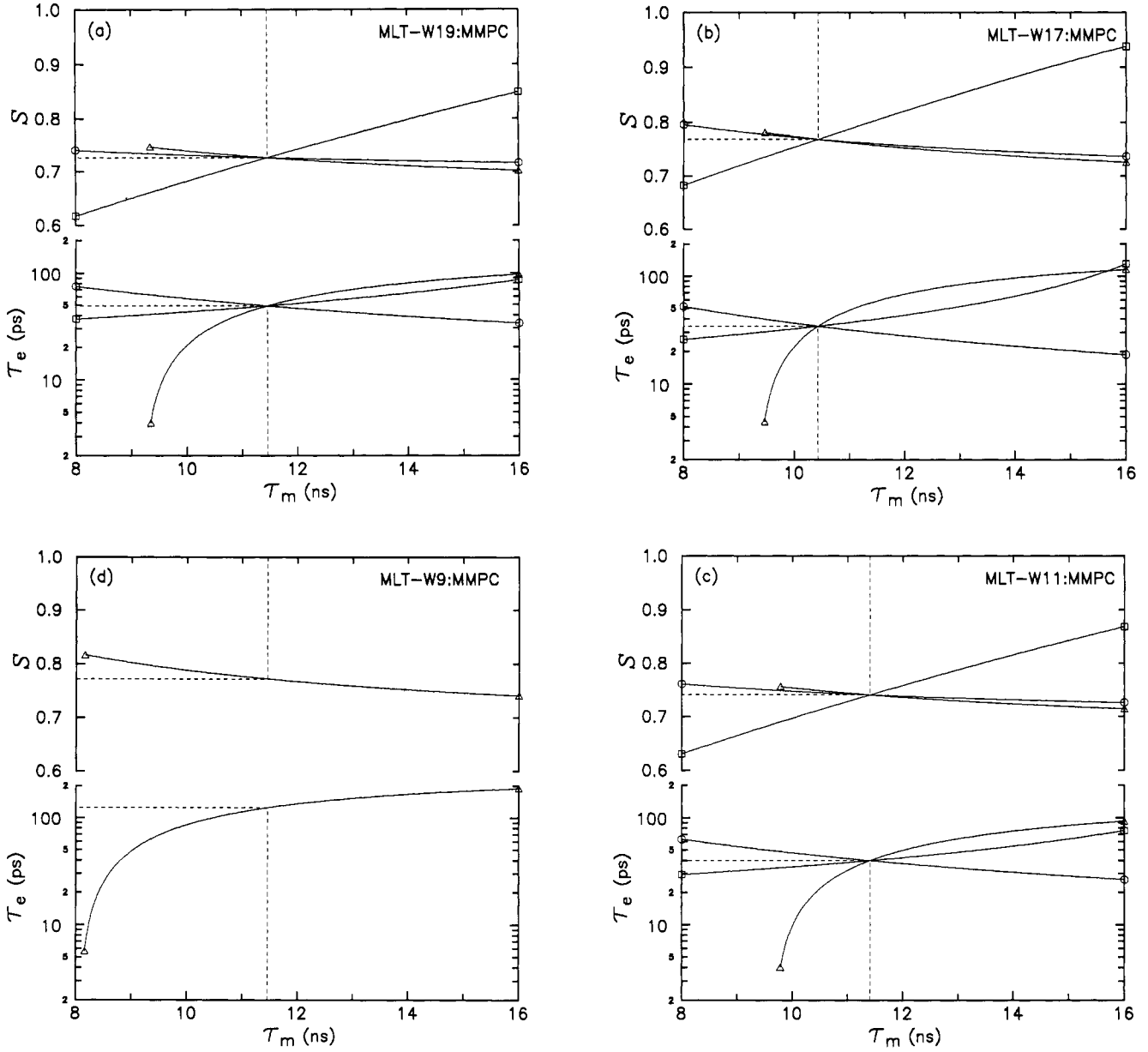

FIGURE 4: Tryptophan side chain dynamics in the micelle-bound MLT peptides determined from combined ^{13}C NMR, mean fluorescence lifetime, and steady-state fluorescence anisotropy data. T_1–NOE (□), T_1–$\bar{r}$ (△), and/or NOE–$\bar{r}$ (○) curves intersect to give motional parameter values characterizing the amplitude (order parameter, S) and rate ("effective" correlation time, τ_e) of Trp side chain motion and overall correlation time (τ_m) for the peptide–micelle complex. (a) MLT-W19/MMPC; (b) MLT-W17/MMPC; (c) MLT-W11/MMPC; (d) MLT-W9/MMPC. A T_1–$\bar{r}$ curve only is drawn for micelle-bound MLT-W9 (see text).

apolar environment, probably among lipid acyl chains; (4) MLT-W17 and MLT-W19 show similar and less extreme behavior than the other analogues, i.e., they have intermediate helix-forming ability in the presence of phospholipid substrates, show moderate perpendicular orientational order in lipid bilayer films, and their Trp side chains are probably located at the lipid–water interface of the micellar or bilayer structure.

Dynamics of the Lipid-Bound Peptides

Tryptophan Side Chain Dynamics. Incorporation of [$^{13}C\delta_1$]Trp into each of the MLT peptides allows, under appropriate experimental conditions, steady-state fluorescence anisotropy and fluorescence lifetime data to be used in conjunction with ^{13}C NMR relaxation data to extract values for parameters descriptive of Trp side chain and peptide backbone motion. Specifically, T_1–NOE, T_1–$\bar{r}$, and NOE–$\bar{r}$ curves (see Materials and Methods) were generated from NMR and fluorescence data to quantitate Trp side chain mobility in terms of a "generalized order parameter" S and an effective local correlation time τ_e. An overall correlation time for the macromolecule (in this case, for peptide–micelle complexes), τ_m, is also obtained when T_1, NOE, and fluorescence data are all available. Analysis of the NMR data alone essentially follows the "model-free" approach of Lipari and Szabo (1982a,b) as adapted by Weaver et al. (1989b) for the concomitant use of NMR and fluorescence data to assess Trp side chain dynamics.

In Figure 4, S versus τ_m and τ_e versus τ_m plots are shown for each of the micelle-bound MLT peptides. T_1–NOE, T_1–$\bar{r}$, and NOE–$\bar{r}$ curves are shown for MLT-W19, MLT-W17, and MLT-W11. The common intersection of these two-parameter curves furnishes a "unique" solution for the motional variables, S and τ_e, describing the dynamics of the Trp side chain and provides a value for τ_m, the overall correlation time of the peptide–micelle complex (for numerical data, see Table III). A T_1–$\bar{r}$ curve only is drawn for MLT-W9 because its measured NOE was lower than the theoretical minimum NOE under the experimental conditions. This problem brings up the issue

of experimental error in the NMR and fluorescence observables.

In our studies, we found T_1 to generally be the most accurately measurable (±5%) of the ^{13}C NMR relaxation parameters, followed by the NOE (±10%), then T_2 (±20%). Steady-state fluorescence anisotropy values can be measured very accurately as can mean fluorescence lifetimes (both within 1 or 2%). It should also be noted that motional parameters determined from NMR and fluorescence data were found to depend strongly on values chosen for r_0 and $\Delta\delta$ in the case of Trp side chain dynamics. These values should either be known *a priori* or determined with considerable care (see Materials and Methods). By contrast, due to the relatively small $\Delta\delta$ value for the saturated Gly12 Cα, peptide chain dynamics showed very little dependence on chemical shift anisotropy. As a consequence of such considerations, T_1–$\bar{r}$ curves should allow the most accurate evaluation of Trp side chain dynamics when a reasonably good experimental or theoretical estimate for the overall correlation time is also available.

Are the observed τ_m values determined from combined, T_1, NOE, and $\bar{r}$ data physically reasonable? Assuming that the overall rotational diffusion of the various MLT peptide–micelle complexes is similar (a function of micellar weight and shape), then τ_m values for all MLT peptide–micelle complexes should be approximately equal. Indeed, observed overall correlation times are quite similar for MLT-W19, MLT-W17, and MLT-W11 (Table III). How do these observed peptide–micelle correlation times compare with theoretical values? In two-dimensional DMPC crystals, the phosphocholine head group occupies a cross-sectional area of 65.2 Å^2, and the bilayer thickness is 34.5 Å (Lis et al., 1982). Assuming comparable dimensions for the lysolipid monomer, a spherical MMPC micelle modeled as a collection of conically shaped lipid monomers would have a radius 17.3 Å; the solid angle per lipid molecule is $65.2/17.3^2 = 0.219$ steradians. Thus, the number of MMPC monomers per micelle[4] is given by $4\pi/0.219 \simeq 57$, and the anhydrous micellar weight is $57 \times 467.6 \simeq 26\,830$ Da. Assuming a hydrated specific volume of 0.95 cm^3 g^{-1} (Haberland & Reynolds, 1975), by the Stokes–Einstein–Debye relation one can estimate the rotational correlation time for a spherical MMPC micelle in water at 20 °C to be 10.5 ns. If one adds the molecular weight of a *single* MLT peptide to the micellar weight, the predicted τ_m for the peptide–micelle complex becomes 11.6 ns. This value agrees remarkably well with the observed τ_m values of 11.5, 10.4, and 11.4 ns, respectively, for micelle-bound MLT-W19, MLT-W17, and MLT-W11.[5] We note that hydrodynamic characterization of MLT–dodecylphosphocholine (C12) mixed micelles by Lauterwein et al. (1979) revealed a correlation time of ~10 ns and a peptide to lipid stoichiometry of 1.1 peptides bound per micelle. The experimental hydrodynamic data are thus consistent with the binding of a *single* MLT peptide per phosphocholine micelle. If, however, MLT is capable of forming a lipid-bound oligomer in lipid *vesicles*, then one must conclude that such a species is structurally incompatible with the *micellar* lipid environment since a micelle-bound oligomer is not observed experimentally.

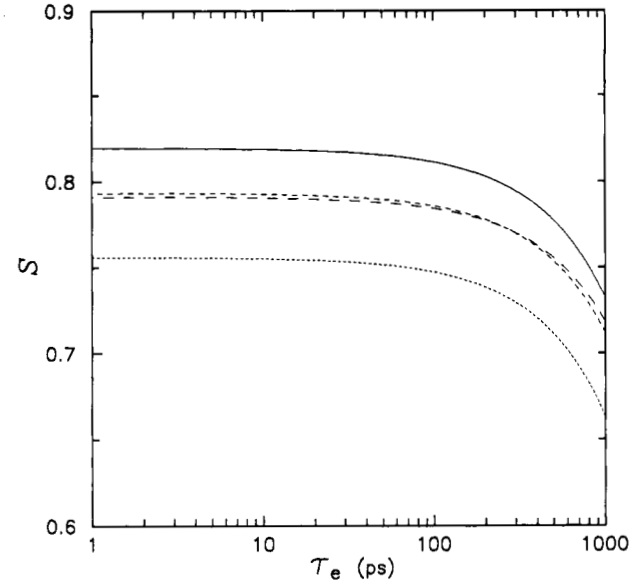

FIGURE 5: Tryptophan side chain dyanmics in MLT peptide/DMPC vesicle complexes. Order parameter (S) and effective correlation times (τ_e) consistent with mean fluorescence lifetime and steady-state fluorescence anisotropy data are determined from eq 3, assuming an overall correlation time, τ_m, of 746 ns for small unilamellar DMPC vesicles. MLT-W19 (——), MLT-W17 (— —), MLT-W11 (– – –), and MLT-W9 (- - -).

Having concluded that the peptide–micelle τ_m values are physically reasonable, one can begin to interpret the corresponding S and τ_e values for the Trp side chain of the respective micelle-bound peptides. Effective correlation times for the local motion of the Trp side chain are quite short: τ_e = 34–49 ps, *except* for MLT-W9, where τ_e = 123 ps. The low picosecond values compare very well with correlation times of 35–45 ps measured by anisotropic absorption of free tryptophan in water (Chen et al., 1988). One can thus argue that the Trp side chain of micelle-bound MLT-W19, MLT-W17, and MLT-W11 suffers no loss of mobility in terms of its local motional *rate* compared with free solution. By contrast, the longer correlation time for the MLT-W9 Trp side chain implies either some degree of viscous drag due to a deeper partitioning among micellar acyl chains or concerted motion of the indole moiety *and* an attached peptide segment. Order parameter values of 0.73 and 0.74 were measured for MLT-W19 and MLT-W11, respectively. S values of 0.77 for both MLT-W17 and MLT-W9 are not significantly larger. These S values correspond to an indole ring flip angle (ϕ_0) of between ±50° and ±44° about the β–γ bond of the Trp side chain (eq 9). It should be reiterated that τ_e and S values need not be correlated. A constrained *rate* of side chain motion does not necessarily imply similar constraints on the *amplitude* of side chain motion, or vice-versa. This situation apparently pertains to the interpretation of MLT-W9 dynamics when compared with the other micelle-bound peptides.

How do micellar Trp dynamics compare with Trp side chain mobility in the DMPC-bound MLT peptides? Fluorescence data only were obtained for the MLT peptides bound to DMPC vesicles. NMR data could not be obtained due to line broadening of the ^{13}C peptide resonances. This observation is consistent with a much longer overall correlation time for DMPC vesicles. By the Stokes–Einstein–Debye relation, τ_m = 746 ns, based on an aggregate molecular weight of 1.93×10^6 Da and a hydrated specific volume of 0.973 cm^3 g^{-1} at 30 °C (Watts et al., 1978). Figure 5 shows S versus τ_e plots generated from eq 3 for the MLT peptide–DMPC complexes

[4] Calculation of the micellar aggregate number follows that of Saunders et al. (1966) for lysophosphatidylcholine and is in general agreement with aggregate numbers typical of C12–C15 lysolipids [cf. Tanford (1981)].

[5] Since a reliable NOE value was not available for MLT-W9, only the T_1–$\bar{r}$ curve is plotted in Figure 4. In this case, the available data are insufficient to uniquely determine τ_m. A τ_m value equal to that observed for the micelle-bound MLT-W11 (11.4 ns) was therefore assigned to the MLT-W9–MMPC complex in order to extract comparative S and τ_e values for the Trp9 side chain.

given this τ_m value. For τ_e values below ~300 ps, order parameter values remain essentially constant, ranging from 0.72 to 0.82 for all of the MLT peptide–DMPC vesicle complexes. *If* similar τ_e values obtain in DMPC and MMPC lipid environments, S values for the DMPC-bound peptides would therefore be nearly equal to (MLT-W9) or somewhat larger (remaining analogues) than those observed in MMPC preparations. Conversely, if order parameters were constrained to be equal in DMPC- and MMPC–peptide complexes, then τ_e values would *not* approximate values observed for the MLT peptide–micelle complexes (Figure 5). Although we favor the former interpretation (higher S values and comparable τ_e's in DMPC relative to MMPC), in the absence of additional experimental data, one cannot unambiguously characterize Trp side chain dynamics from the fluorescence data alone.

Peptide Chain Dynamics. T_1–NOE curves are plotted in Figure 6 for the Gly12 $^{13}C\alpha$ resonance of micelle-bound MLT-W17 and MLT-W11. Curves are not drawn for MLT-W9 and MLT-W19 since observed NOE values were less than the theoretical minimum value for the NOE, presumably due to measurement uncertainty (see Table III). Motional parameters for the peptide chain Gly12 Cα were determined from the curves using τ_m values already determined from analyses of Trp dynamics. Order parameter values of 0.72 and 0.76 calculated for MLT-W17 and MLT-W11, respectively, are remarkably similar to Trp side chain S values. Peptide chain correlation times of 29 and 23 ps, respectively, for MLT-W17 and MLT-W11, imply very rapid local or segmental motion of the peptide chain in the vicinity of Gly12, perhaps characteristic of backbone atoms in α-helix structure.

If the "effective" correlation time, τ_e, is thought of as a time constant reflecting the "effective" mass of the molecular segment (i.e., side chain, peptide chain segment, protein subdomain, etc.) to which a ^{13}C label and/or fluorophore is attached, then one can rationalize how S values for intrapeptide "segmental" motions might be similar in the micellar environment, while τ_e values differ. The similarity of Trp side chain and Gly peptide chain order parameters suggests that values of 0.7–0.8 characterize the "average" degree of steric hindrance experienced by the indole ring or peptide chain in the very fluid, dynamic medium of the lysolipid micelle. The Trp side chain and Gly Cα may thus sample similar steric environments over the time scale characteristic of micellar phospholipid motions. In other words, peptide τ_e values even as short as tens of picoseconds may be long relative to the motional time scale for individual micellar lipids. By the Stokes–Einstein–Debye relation, effective correlation times of 35–45 ps observed for MLT-W19, MLT-W17, and MLT-W11 Trp Cδ_1–H motion in the micellar environment are consistent with motion of an independent molecular "segment" with a mass of 90–115 Da, essentially that of the indole ring (116 Da). The τ_e value for micelle-bound MLT-W9 (123 ps) corresponds to collective motion of a somewhat larger molecular segment of 315 Da, perhaps that of the "buried" indole ring and an attached peptide chain segment. Finally, the Gly12 Cα τ_e values of ~25 ps are physically consistent with concerted motion of a rather short 64-Da chain segment, perhaps the set of coplanar atoms comprising a single peptide bond adjacent to a glycyl residue (68 Da).

Conclusions

Upon binding to MMPC or DMPC lipid substrates, all of the MLT peptides clearly become relatively more α-helical. The extent of helicity depends on the intrinsic helix-forming potential of the peptide, which, in turn, is dictated by the peptide sequence. From the apparent intramolecular

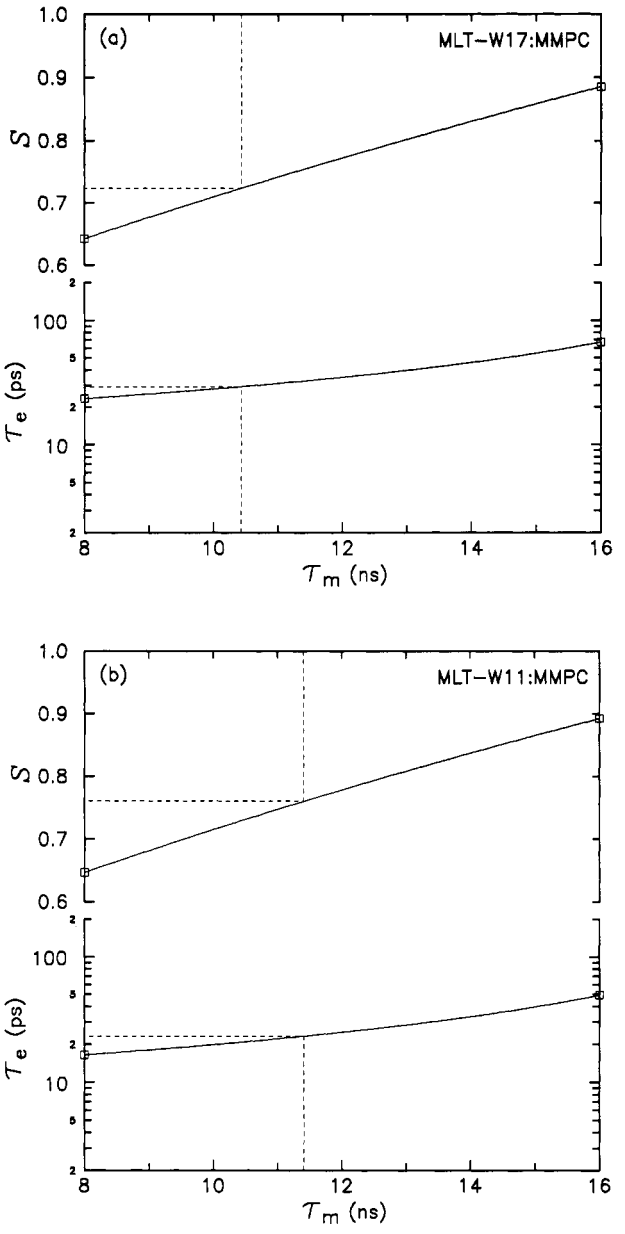

FIGURE 6: Peptide chain (Gly12 Cα) dynamics of micelle-bound MLT peptides determined from ^{13}C NMR T_1–NOE data. The dashed lines indicate predicted S and τ_e values assuming overall correlation times of (a) 10.4 ns for MLT-W17/MMPC micelles, and (b) 11.4 ns for MLT-W11/MMPC micelles (see text).

fluorescence quenching and the NMR chemical shift data, we infer an intact helical segment extending at least from Lys7 to Gly12; fractional helicity values from CD and ATR–FTIR data support helical segments involving at least 28% and up to 91% of MLT peptide residues. In MMPC micelles, the peptides are minimally ~50% α-helical. Hydrophobic moment calculations suggest that these peptides become less amphiphilic as one moves toward the C-terminus (Figure 3). If, as seems reasonable, interaction with a lipid substrate stabilizes a nascent amphiphilic helix, then the N-terminal "half" of the MLT sequence may constitute the 25–50% "core" of α-helical residues. For those residues involved in α-helical structure, ATR–FTIR measurements reveal a greater degree of orientational order perpendicular to the plane of the lipid bilayer for all of the MLT peptides, except MLT-W9. Although MLT-W9 becomes 62% α-helical in MMPC micelles, insertion of the N-terminal helix in *any* preferred orientation relative to the bilayer plane (perpendicular or not) may be hindered by the bulky Trp9 side chain. This hypothesis does not,

however, preclude insertion of the Trp9 side chain itself well into the apolar lipid environment; the MLT-W9 N-terminal helix may, for steric or energetic reasons, simply adopt a wider variety of lipid-bound orientations than the other MLT peptides. A structural model emerges for MLT as interacting with a lipid substrate through an N-terminal α-helix which, unless sterically or dynamically hindered, assumes an orientation perpendicular to the bilayer plane.

Do the dynamics of the micelle-bound peptides support this structural model? If so, can one propose a mechanism for MLT-induced membranolysis consistent with peptide structure and dynamics? First, MLT peptide–lipid micelle correlation times are consistent with binding of a *single* MLT peptide monomer per micelle. Second, the distinct structural, dynamic, and lytic behavior of the lipid-bound peptides, especially MLT-W9, suggests a central role for the N-terminal peptide segment in any membranolytic mechanism. The Trp9 side chain of MLT-W9 appears to be relatively motionally constrained (longer τ_e) in comparison with Trp mobility in the other micelle-bound peptides. This observation is again consistent with partitioning of the N-terminal segment of this peptide farther into the micellar acyl chain environment than the remainder of the peptide. Interestingly, the kinetics of MLT-W9 cytolysis are much slower than those of MLT-W19, MLT-W17, and MLT-W11 (Weaver et al., 1989a). Introduction of a bulky aromatic side chain into the N-terminal helical peptide segment may impair the *dynamics* of its insertion into the membrane. Indeed, regions of enhanced flexibility appear to be important for efficient functioning of signal peptides (Gennity et al., 1990). If motional flexibility of amino acid side chains and efficient bilayer penetration by the N-terminal α-helical segment of MLT are related, then the slowed motional rate of the MLT-W9 Trp side chain may reveal a connection between peptide dynamics and cytolytic activity.

Several experimental observations and considerations also contribute to a mechanism proposed below for MLT-induced membranolysis: (1) Pro14 is not essential for MLT function (DeGrado et al., 1982; Dempsey et al., 1991); this rules out a purely static membranolytic mechanism based on structural incompatibility of a 'bent' α-helical peptide with the membrane bilayer; (2) ^{2}H NMR studies indicate that positively charged MLT C-terminal residues perturb phosphocholine head group packing (Beschiaschvili & Seelig, 1990); (3) peptides corresponding to MLT residues 1–13 and 15–26 are not lytic individually or in concert (Prendergast et al., unpublished observations); (4) unlike "native" MLT-W19, the MLT analogues do not become tetrameric nor do they form discrete oligomeric species in aqueous solution, yet they retain lytic activity (Weaver et al., 1989a); (5) nonspecifically aggregated aqueous MLT-W9 dissociates on binding to MMPC micelles.

The cumulative structural, dynamic, and functional data for MLT and the analogues described here favor a membranolytic mechanism in which MLT acts as a monomeric α-helical peptide electrostatically anchored through its C-terminal residues to one face of the membrane and of insufficient length to "translocate" a relatively flexible N-terminal signal-peptide-like helical segment completely through the bilayer. In fact, MLT resembles a "reverse-sequence" signal peptide, having highly basic residues near its C-terminus and a hydrophobic segment extending to the peptide N-terminus. Like precursor signal sequences, we believe that a "loop model" also applies for MLT insertion into the membrane, i.e., positively charged peptide side chains interact with phospholipid acidic groups followed by insertion of the remainder of the peptide as a folded or loop structure (Inouye & Halegoua, 1980). Indeed, ^{1}H NMR studies suggest that residues 1–12 and 16–26 of micelle-bound MLT constitute distinct α-helical "domains" separated by a relatively flexible intervening segment (Brown & Wüthrich, 1981). A more recent 2D ^{1}H NMR and distance geometry analysis of micelle-bound MLT is also consistent with an α-helical bent rod conformation for the lipid-bound peptide (Inagaki et al., 1989; Ikura et al., 1991). As an *amphiphilic* α-helix folded upon itself in such a way so as to partially internalize or protect its hydrophilic face, MLT would initially expose hydrophobic side chains only to membrane phospholipid acyl chains. This transient folded conformation would facilitate initiation of peptide translocation.

In a subsequent stage of peptide translocation, however, we speculate that *unfolding* (i.e., separation of the N- and C-terminal helical domains) of the incompletely translocated peptide results in exposure of MLT hydrophilic side chains to the hydrophobic interior of the bilayer. This situation contrasts with intramembrane exposure of more uniformly hydrophobic side chains characteristic of signal peptide sequences. The structural compromise of the cis membrane leaflet would allow water to penetrate along the hydrophilic surface of the "wedge" or V-shaped peptide. Interaction of MLT and MLT-like peptides with the membrane bilayer would thus constitute an incomplete or "abortive" translocation event; the peptide N-terminal helix does not (and structurally cannot) reach the trans side of the bilayer. The energetic cost of the abortively translocated amphiphilic peptide helix exceeds the predominantly entropically driven (hydrophobic) stabilization of the membrane bilayer. The net result is catastrophic curvature of the membrane due to local micellization and *non*osmotic membranolysis.

Finally, we note that amino acid residues in the N-terminal segment of MLT should allow for substantial motional freedom of the N-terminal helix within the membrane bilayer thereby facilitating its (abortive) translocation. A bulky residue (e.g., Trp9) attached to the N-terminal helical segment might sterically or dynamically interfere with initiation of helix translocation and thus explain its reduced cytolytic rate. In sum, hydrophobic forces provide the driving force for the proposed membranolytic mechanism; peptide helix amphiphilicity is important, but it is not the whole story: structural mismatching of helix length and membrane thickness may "potentiate" the membranolytic event; side chain and backbone mobility may facilitate initiation of MLT translocation.

Elucidation of a detailed molecular mechanism for MLT-induced membranolysis requires experiments designed to probe just what portions of the lipid acyl chains contact peptide amino acid side chains and to what extent the lipid acyl chains influence peptide side chain and backbone dynamics (and vice versa). Independent confirmation of Trp side chain τ_e values derived from NMR and steady-state fluorescence experiments would provide quantitative validation of the results presented here. Time-resolved fluorescence anisotropy experiments are now underway on related peptides (P. Buckley, personal communication). In particular, future studies will focus on elucidation of the structure and dynamics of residues closer to the peptide N-terminus in MLT–lipid complexes. Definitive localization of MLT N-terminal residues at or near the cis versus trans membrane leaflet will be especially important for determining the actual "lytic" conformation(s) of membrane-bound MLT monomer.

ACKNOWLEDGMENTS

This paper is taken in part from the doctoral thesis of A.J.W.

References

Abragam, A. (1961) *The Principles of Nuclear Magnetism*, Oxford University Press, London.

Altenbach, C., & Hubbell, W. L. (1988) *Proteins 3*, 230–242.

Altenbach, C., Froncisz, W., Hyde, J. S., & Hubbell, W. L. (1989) *Biophys. J. 56*, 1183–1191.

Batenburg, A. M., & de Kruijff, B. (1988) *Biosci. Rep. 8*, 299–307.

Beschiaschvili, G., & Seelig, J. (1990) *Biochemistry 29*, 52–58.

Brauner, J. W., Mendelsohn, R., & Prendergast, F. G. (1987) *Biochemistry 26*, 8151–8158.

Brown, L. R. (1979) *Biochim. Biophys. Acta 557*, 135–148.

Brown, L. R., & Wüthrich, K. (1981) *Biochim. Biophys. Acta 647*, 95–111.

Byler, D. M., & Susi, H. (1986) *Biopolymers 25*, 469–487.

Chandani, B., & Balasubramanian, D. (1986) *Biopolymers 25*, 1259–1272.

Chen, L. X.-Q., Engh, R. A., & Fleming, G. R. (1988) *J. Phys. Chem. 92*, 4811–4816.

Dawson, C. R., Drake, A. F., Helliwell, J., & Hider, R. C. (1978) *Biochim. Biophys. Acta 510*, 75–86.

DeGrado, W. F., Musso, G. F., Lieber, M., Kaiser, E. T., & Kezdy, F. J. (1982) *Biophys. J. 37*, 329–338.

Dempsey, C. E., Bazzo, R., Harvey, T. S., Syperek, I., Boheim, G., & Campbell, I. D. (1991) *FEBS Lett. 281*, 240–244.

Drake, A. F., & Hider, R. C. (1979) *Biochim. Biophys. Acta 555*, 371–373.

Dill, K., & Allerhand, A. (1979) *J. Am. Chem. Soc. 101*, 4376–4378.

Eisenberg, D., Weiss, R. M., & Terwilliger, T. C. (1984) *Proc. Natl. Acad. Sci. U.S.A. 81*, 140–144.

Fraser, R. D. B. (1953) *J. Chem. Phys. 21*, 1511–1515.

Gennity, J., Goldstein, J., & Inouye, M. (1990) *J. Bioenerg. Biomembr. 22*, 233–269.

Georghiou, S., Thompson, M., & Mukhopadhyay, A. K. (1982) *Biophys. J. 37*, 159–160.

Gierasch, L. M., Lacy, J. E., Thompson, K. F., Rockwell, A. L., & Watnick, P. I. (1982) *Biophys. J. 37*, 275–284.

Haberkorn, R. A., Stark, R. E., van Willigen, H., & Griffen, R. G. (1981) *J. Am. Chem. Soc. 103*, 2534–2539.

Haberland, M. E., & Reynolds, J. A. (1975) *J. Biol. Chem. 250*, 6636–6639.

Harrick, N. J. (1979) *Internal Reflection Spectroscopy*, Harrick Scientific, Ossining, NY.

Hermetter, A., & Lakowicz, J. R. (1986) *J. Biol. Chem. 261*, 8243–8248.

Ikura, T., Gō, N., & Inagaki, F. (1991) *Proteins 9*, 81–89.

Inagaki, F., Shimada, I., Kawaguchi, K., Hirano, M., Terasawa, I., Ikura, T., & Gō, N. (1989) *Biochemistry 28*, 5985–5991.

Inouye, M., & Halegoua, S. (1980) *CRC Crit. Rev. Biochem. 7*, 339–371.

John, E., & Jähnig, F. (1988) *Biophys. J. 54*, 817–827.

Kinosita, K., Kawato, S., & Ikegami, A. (1977) *Biophys. J. 20*, 289–305.

Knoppel, E., Eisenberg, D., & Wickner, W. (1979) *Biochemistry 18*, 4177–4181.

Kubota, S., & Yang, J. T. (1986) *Biopolymers 25*, 1493–1504.

Lauterwein, J., Bosch, C., Brown, L. R., & Wüthrich, K. (1979) *Biochim. Biophys. Acta 556*, 244–264.

Lipari, G., & Szabo, A. (1982a) *J. Am. Chem. Soc. 104*, 4546–4559.

Lipari, G., & Szabo, A. (1982b) *J. Am. Chem. Soc. 104*, 4559–4570.

Lis, L. J., McAlister, M., Fuller, N., Rand, R. P., & Parsegian, V. A. (1982) *Biophys. J. 37*, 667–665.

McKnight, C. J., Briggs, M. S., & Gierasch, L. M. (1989) *J. Biol. Chem. 264*, 17293–17297.

Meiboom, S., & Gill, D. (1958) *Rev. Sci. Instrum. 29*, 688–691.

Mendelsohn, R., & Mantsch, H. H. (1986) in *Progress in Protein–Lipid Interactions* (Watts, A., & De Pont, J. J. H. H. M., Eds.) 2nd ed., pp 103–146, Elsevier, Amsterdam.

Nabedryk, E., Gingold, M. P., & Breton, J. (1982) *Biophys. J. 38*, 243–249.

Quay, S. C., & Tronson, L. P. (1983) *Biochemistry 22*, 700–707.

Ruggiero, A. J., Todd, D. C., & Fleming, G. R. (1990) *J. Am. Chem. Soc. 112*, 1003–1014.

Saunders, L. (1966) *Biochim. Biophys. Acta 125*, 70–74.

Schiffer, M., & Edmundson, A. B. (1967) *Biophys. J. 7*, 121–135.

Shindo, H., Egan, W., & Cohen, J. S. (1978) *J. Biol. Chem. 253*, 6751–6755.

Snyder, R. G., Strauss, H. L., & Elliger, C. A. (1982) *J. Phys. Chem. 86*, 5145–5150.

Stafford, R. E., Fanni, T., & Dennis, E. A. (1989) *Biochemistry 28*, 5113–5120.

Strom, R., Podo, F., Crifò, C., & Zaccai, G. (1982) *Adv. Exp. Med. Biol. 148*, 195–207.

Surewicz, W. K., Moscarello, M. A., & Mantsch, H. H. (1987) *Biochemistry 26*, 3881–3886.

Talbot, J. C., La Lanne, J., Faucon, J.-F., & Dufourcq, J. (1982) *Biochim. Biophys. Acta 689*, 106–112.

Tanaka, F., & Mataga, N. (1987) *Biophys. J. 51*, 487–495.

Tanford, C. (1981) *The Hydrophobic Effect: Formation of Micelles and Biological Membranes*, J. Wiley & Sons, New York.

Terwilliger, T. C., & Eisenberg, D. (1982a) *J. Biol. Chem. 257*, 6010–6015.

Terwilliger, T. C., & Eisenberg, D. (1982b) *J. Biol. Chem. 257*, 6016–6022.

Tosteson, M. T., & Tosteson, D. C. (1981) *Biophys. J. 36*, 109–116.

Vogel, H., & Jähnig, F. (1986) *Biophys. J. 50*, 573–582.

Vogel, H., & Rigler, R. (1987) in *Structure, Dynamics and Function of Biomolecules* (Ehrenberg, A., Rigler, R., Nilsson, L., & Gräslund, A., Eds.) pp 289–294, Springer, Berlin.

Vogel, H., Jähnig, F., Hoffmann, V., & Stümpel, J. (1983) *Biochim. Biophys. Acta 733*, 201–209.

Watts, A., Marsh, D., & Knowles, P. F. (1978) *Biochemistry 17*, 1792–1801.

Weaver, A. J., Kemple, M. D., & Prendergast, F. G. (1989a) *Biochemistry 28*, 8614–8623.

Weaver, A. J., Kemple, M. D., & Prendergast, F. G. (1989b) *Biochemistry 28*, 8624–8639.

Yunes, R. A. (1982) *Arch. Biochem. Biophys. 216*, 559–565.